Journal of Power Sources 225 (2013) 192–199

Contents lists available at SciVerse ScienceDirect

Journal of Power Sources

journal homepage: www.elsevier.com/locate/jpowsour

Effect of carbon nanofiber surface functional groups on oxygen reduction in alkaline solution

Ren-Sheng Zhong [a], Yuan-Hang Qin [a], Dong-Fang Niu [a,*], Jing-Wei Tian [a], Xin-Sheng Zhang [a,*], Xin-Gui Zhou [a], Shi-Gang Sun [b], Wei-Kang Yuan [a]

[a] State Key Laboratory of Chemical Engineering, East China University of Science and Technology, Shanghai 200237, China
[b] State Key Laboratory of Physical Chemistry of Solid Surfaces, Xiamen University, Xiamen 361005, China

HIGHLIGHTS

- Different surface functional groups were successfully imported onto CNF surface.
- CNF–ON exhibited the highest ORR activity, followed by CNF–OX, CNF–CO and CNF–OH.
- CNF–ON could catalyze ORR through the $4e^-$ pathway.

ARTICLE INFO

Article history:
Received 30 July 2012
Received in revised form
11 October 2012
Accepted 12 October 2012
Available online 23 October 2012

Keywords:
Oxygen reduction reaction
Electrocatalyst
Carbon nanofiber
Surface functional groups

ABSTRACT

Carbon nanofibers (CNFs) with different content of surface functional groups which are carboxyl groups (CNF–OX), carbonyl groups (CNF–CO) and hydroxyl groups (CNF–OH) and nitrogen-containing groups (CNF–ON) are synthesized, and their electrocatalytic activities toward oxygen reduction reaction (ORR) in alkaline solution are investigated. The result of X-ray photoelectron spectroscopy (XPS) characterization indicates that a higher concentration of carboxyl groups, carbonyl groups and hydroxyl groups are imported onto the CNF–OX, CNF–CO and CNF–OH, respectively. Cyclic voltammetry shows that both the oxygen- and nitrogen-containing groups can improve the electrocatalytic activity of CNFs for ORR. The CNF–ON/GC electrode, which has nitrogen-containing groups, exhibits the highest current density of ORR. Rotating disk electrode (RDE) characterization shows that the oxygen reduction on CNF–ON/GC electrode proceeds almost entirely through the four-electron reduction pathway, the CNF–OX/GC, CNF–CO/GC and CNF–OH/GC electrodes proceed a two-electron reduction pathway at low potentials (−0.2 V to −0.6 V) followed by a gradual four-electron reduction pathway at more negative potentials, while the untreated carbon nanofiber (CNF–P/GC) electrode proceeds predominantly by a two-electron reduction pathway within the whole range of potential studied.

1. Introduction

Recently, intensive attention has been paid to CNFs due to their outstanding structural, mechanical, and extraordinary electrical properties [1,2]. CNFs can be utilized for a variety of promising applications, such as, structural and functional composites, and they are also widely used as catalyst support in fuel cells because of their low cost, long cycle life and high electrical conductivity [3]. Studies have shown that metal nanoparticles supported on CNFs provide much improvement in catalytic activity [4,5]. Platelet CNF (p-CNF) has a stronger interaction with Pd nanoparticles and the electrocatalyst supported on p-CNF exhibits a higher electrochemical surface area and more positive onset reduction potential of oxygen reduction reaction than that supported on activated carbon [6].

CNFs are also considered to be promising candidates for the ORR catalysts in alkaline fuel cells due to their high surface area, high chemical and thermal stability and high electrical conductivity [7,8]. Before being used as catalysts, the CNFs are usually oxidized to introduce oxygen-containing surface groups to increase the active sites. Many studies have shown that the oxygen-containing surface groups formed on CNF are closely related to the oxidation methods, while air oxidation and acid oxidation are the frequently used methods [9]. Air oxidation treatment preferentially forms hydroxyl and carbonyl groups, while acid treatment forms carboxylic acid

* Corresponding authors. Tel.: +86 21 64253469; fax: +86 21 64253528.
E-mail addresses: dfniu@ecust.edu.cn (D.-F. Niu), xszhang@ecust.edu.cn (X.-S. Zhang).

0378-7753/$ – see front matter © 2012 Elsevier B.V. All rights reserved.
http://dx.doi.org/10.1016/j.jpowsour.2012.10.043

groups on the surface of CNF [10,11]. Intensive efforts have been devoted on the N-doped carbon materials due to their high electrocatalytic activity and low overpotential. Several methods can be employed to synthesize N-doped carbon nanotubes, such as, arc-discharge [12], laser ablation [13], modified chemical vapor deposition (CVD) methods [14,15] and high temperature pyrolysis [16].

The ORR plays a significant role in controlling the performance of the cathode in a fuel cell, and efficient ORR electrocatalysts are essential for the practical applications of the fuel cells [17,18]. The reduction of oxygen at carbon based electrodes has been extensively studied [19,20]. The ORR proceeds through either a four-electron pathway producing water as the end product, or a two-electron pathway producing hydrogen peroxide as the intermediate [21,22]. The electrocatalytic activity towards ORR is not only depended on the microstructure, such as the edge plane and the basal plane of the CNFs [23], but also significantly determined by the surface functional groups, such as oxygen-containing groups [24] and nitrogen-containing groups [25]. Xu et al. [26] examined the reduction of oxygen on several carbon surfaces and found the oxygen-containing groups could improve the proton transfer rate. Qu et al. [25] synthesized a nitrogen-doped graphene (N-graphene) by chemical vapor deposition using NH_3 as the nitrogen source, and found the N-graphene electrode could act as a metal-free ORR catalyst via a four-electron pathway in alkaline fuel cells. However, it remains unclear that which type of functional groups plays the major role towards ORR.

In this paper, we studied the relationship between the types of surface functional groups and their electrocatalytic activity towards ORR in alkaline solution. Different treating methods were used to introduce the oxygen-containing surface groups onto CNFs, and the properties of surface functional groups on the modified CNFs were studied by XPS. The effects of different types of surface functional groups on the catalytic activity toward ORR were evaluated by cyclic voltammetry (CV) experiment. Rotating disk electrode technology was applied to investigate the ORR mechanism on CNF catalysts.

2. Experimental

2.1. Surface modifications of carbon nanofibers

The acid-treated CNF was achieved by sonochemical treatment [2,27]. Typically, the surface treatment process was as follows: 2.0 g of fishbone CNFs (f-CNFs, 95% purity from Shenzhen Nanotech Port Co., Ltd) were sonochemically treated in a mixed acid solution containing concentrated HNO_3 (188 mL), concentrated H_2SO_4 (160 mL) and ultrapure water (12 mL, 18.2 MΩ cm) in an ultrasonic bath for 2 h at 60 °C. After the surface treatment, the CNFs were filtered and thoroughly washed with ultrapure water before being dried overnight at 120 °C. The acid-treated CNF was denoted as CNF–OX and the untreated CNF was denoted as CNF–P.

The air-treated CNF was achieved through air oxidation performed in a temperature programmed tube furnace [28]. Specifically, 2.0 g of f-CNFs were placed in the tube furnace and heated from 25 °C to 600 °C at a rate of 5 °C min^{-1} under air atmosphere. After the temperature was maintained for 2 h, the furnace was cooled to room temperature slowly. The remaining CNFs were washed with ultrapure water, and then dried at 120 °C overnight. The air-oxidized CNF was denoted as CNF–CO.

Partial conversion of the acidic groups, carboxylic acid groups in particular, on the CNF–OX surface to hydroxyl groups was performed according to the procedure described by Jos van Dillen et al. [29,30]. 0.20 g of lithium aluminum hydride ($LiAlH_4$) was dissolved in 25 ml of fresh anhydrous tetrahydrofuran (THF), while 0.5 g of CNF–OX was dispersed in 50 ml of fresh anhydrous THF. The $LiAlH_4$ suspension was carefully added to the CNF–OX suspension under the nitrogen flow and stirred for 20 h. After the reaction, the mixture was filtrated and washed with anhydrous THF, 0.1 M HCl solution and ultrapure water in series till the filtrate was neutral. The sample was dried at 120 °C overnight and denoted as CNF–OH.

The electrocatalytic activity could be improved by doping the nitrogen atoms into the carbon network according to many reports [25,31]. In this paper, the melamine was used as the nitrogen source to synthesize N-doped CNF (CNF–ON) as reported by Sheng et al. [32]. Briefly, 0.5 g of CNF–OX and 2.5 g of melamine were mixed together by grinding, forming a uniform gray mixture. The mixture in a crucible with a lid was then placed into a corundum tube with nitrogen flow and heated to 700 °C at a rate of 5 °C min^{-1}, and then held for 1 h at 700 °C. The possible doping is that the melamine which was adsorbed on the CNF surface at low temperature, condensed and formed carbon nitride after increasing the temperature, and then the carbon nitride decomposed and doped into graphene layers [32]. The N-doped CNF was denoted as CNF–ON.

2.2. Characterization of carbon catalyst

The textural properties of the modified CNFs were obtained from N_2 adsorption–desorption isotherms (ASAP 2010, Micromeritics, USA) at −196 °C after out-gassing the samples at 190 °C. Specific surface areas were calculated with the Brunauer–Emmett–Teller equation, and the pore volumes and pore size distributions were calculated using the Barrett–Joyner–Halenda (BJH) method. Raman spectroscopy was employed to characterize the functionalized CNFs using a Renishaw InVia Reflex Raman spectrometer with an Ar-ion laser beam at an exciting radiation wavelength of 514.5 nm.

The X-ray photoelectron spectroscopy characterization of CNF was performed using a Kratos AXIS Ultra DLD spectrometer equipped with monochromatic Al Kα radiation at a power of 45 W. To exclude any effects on the values of binding energies due to charging of the sample during the XPS analysis, the data we got were corrected by a linear shift such that the peak maximum of the C1s binding energy of adventitious carbon corresponded to 284.8 eV.

2.3. Electrochemical measurements

Electrochemical measurements were carried out on a PGSTAT 30 electrochemical workstation (Eco Chemie B.V. the Netherlands) and a rotating disk electrode (pine instruments). All experiments were conducted in a three electrode system at 20 ± 1 °C. The working electrode was prepared as follows. A suspension of CNF ink was prepared by ultrasonically dispersing 0.6 mg of CNFs in 90 μl of ethanol and 10 μl of Nafion (5 wt.%) solution for 20 min, and a total of 5 μl of the above solution was carefully pipetted onto a glassy carbon (GC) electrode with 5 mm in diameter, followed by solvent evaporation at room temperature in ambient air for 30 min. An Ag/AgCl (10 wt.% KCl) electrode and a Pt wire were used as the reference and the counter electrodes, respectively. 0.1 M KOH aqueous solution was used as the electrolyte.

3. Results and discussion

3.1. BET and Raman characterizations of CNFs

Table 1 shows the typical textural properties of different treated-CNFs obtained from N_2 adsorption–desorption at cryogenic temperature. The BET surface area is increased after oxidation treatment, which may be due to the more surface groups or an

Table 1
Effect of pre-treatment conditions on the textual properties of CNF.

Sample	BET surface area ($m^2\ g^{-1}$)	Pore volume ($cm^3\ g^{-1}$)	Micropore volume ($cm^3\ g^{-1}$)	Average pore size (nm)
CNF–P	102.03	0.65	0.0058	15.2
CNF–OX	118.99	0.63	0.0048	13.3
CNF–OH	127.03	0.70	0.0036	15.6
CNF–CO	158.38	0.81	0.0081	11.3
CNF–ON	171.46	0.80	0.0078	16.7

increasing surface defects on the CNF surface. Especially for the air oxidation and nitrogen-doped CNF samples, a significant increase from 102.03 $m^2\ g^{-1}$ to 158.38 $m^2\ g^{-1}$ and 171.46 $m^2\ g^{-1}$ respectively, in BET surface area are obtained. The five types of CNFs have apparent mesoporous structure, as their microporous volumes, which range from 0.0036 $cm^3\ g^{-1}$ to 0.0078 $cm^3\ g^{-1}$, are less than 0.01 $cm^3\ g^{-1}$. This may be because the pore structure is mainly formed by the stacking pores between the fibers, so the microstructures and morphology of the treated-CNFs are not seriously damaged by the above modification methods [33].

Raman analysis is a useful tool for providing detailed information about the structure of graphitic materials. The Raman spectra, in the range of Raman shift from 1000 to 2000 cm^{-1}, of the five types of CNFs are showed in Fig. 1. There are two main peaks in the Raman spectrum of CNFs. The first, peak D at about 1350 cm^{-1}, is attributed to disorder structure. The second, peak G at about 1580 cm^{-1}, is attributed to the ordered structure of carbon material. The ratio of the intensity of the D peak to that of the G peak (I_D/I_G) can be used as an indicator of the amount of carbon defect sites due to modification. The I_D/I_G ratio increases slightly upon oxidation treatments for CNFs, ranging from 0.90 to 1.16, respectively. This indicates that these treatments increase the amount of structural defects in the surface of CNF, due to the presence of functional groups on the surface.

3.2. XPS results

XPS experiment has been used to determine the surface groups on CNFs. As shown in Fig. 2, after oxidation treatment, the content of oxygen atoms are significantly increased. Using melamine as nitrogen source, the nitrogen element can be effectively introduced on the CNF–OX by thermal anneal while the content of oxygen

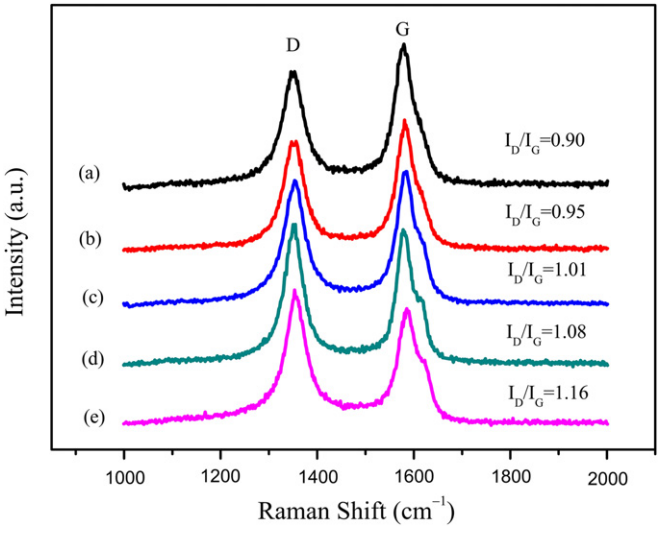

Fig. 1. Raman spectra of CNFs. (a) CNF–P, (b) CNF–OX, (c) CNF–OH, (d) CNF–CO, (e) CNF–ON.

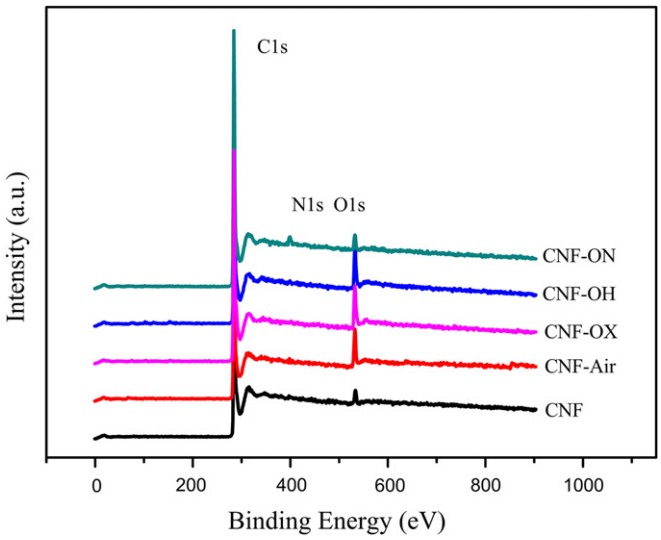

Fig. 2. XPS spectra of CNF with different treatments.

element was decreased. We suggest that the nitrogen doping into CNF frameworks may be ascribed to the CNF surface groups changing from oxygen-containing groups to nitrogen-containing groups to provide active sites.

To better understand the change of the surface properties between the different modifications, the high-resolution C1s XPS spectra of the as-made samples were deconvoluted and five peaks were obtained [34–36]. The main peak (peak 1) is corresponded to sp^2-hybridized graphitic carbon (C–C groups at 284.8 eV). Peak 2, peak 3, peak 4 and peak 5 are attributed to the C–O groups or C=N groups (at 286.0–286.3 eV), C=O groups in carbonyl or quinine groups (at 287.3–287.6 eV), O–C=O groups in carboxyl or ester groups (at 288.8–289.1 eV) and the CO or CO_2 adsorbed on the surface of CNF (at 290.5–291.2 eV), respectively.

Similarly, the high-resolution O1s XPS spectra of the as-made samples also yielded five peaks [11,37]. The peaks are ascribed to the following oxygen groups: Peak I to the carbonyl oxygen of quinines (at 531.0–531.9 eV); peak II to the carbonyl oxygen atoms in esters, anhydrides and oxygen atoms in hydroxyl groups (at 532.3–532.8 eV); peak III to the ether-type oxygen atoms in ester and anhydrides (at 533.1–533.8 eV); peak IV to the oxygen atoms in carboxyl groups (at 534.3–535.4 eV); and peak V has been tentatively ascribed to the H_2O or O_2 adsorbed on the surface of CNF (at 536.0–536.5 eV). The N1s spectra of CNF–ON can be fitted into three peaks at 398.2 eV, 399.5 eV and 401.1 eV, which are corresponded to the pyridine-like nitrogen, pyrrole-like nitrogen and graphitic nitrogen, respectively [16,38]. Fig. 3, Fig. 4 and Fig. 4(d) show typical XPS results together with fitted C1s, O1s and N1s peaks. From Fig. 4(d), we can know that the nitrogen atoms primarily exist in the form of pyridine-like nitrogen.

The results of C1s and O1s peaks are summarized in Table 2 and Table 3, respectively. The concentration of oxygen-containing groups on the CNF surface is slightly different with various treatments according to the XPS spectra and their deconvolution results. For the CNF–CO, a higher intensity of carbonyl groups (peak3, 8.83%) is found in C1s spectra than CNF–OX (5.39%) and CNF–OH (4.03%). which is in good agreement with the O1s results that CNF–CO has a larger peak I (32.37%), assigned to carboxyl groups than CNF–OX (21.47%) and CNF–OH (17.35%). While, in C1s spectra a higher intensity of carboxyl groups is discovered in CNF–OX than that of CNF–CO and CNF–OH, which is in good agreement with the O1s results that CNF–OX has a larger peak IV (24.08%), which

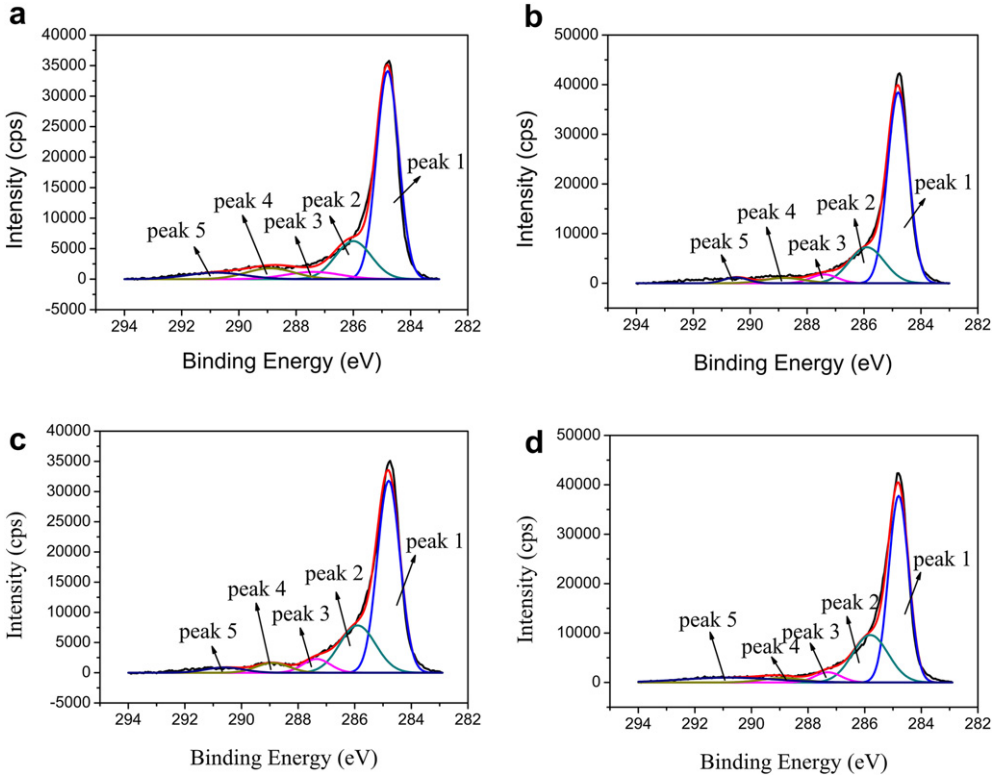

Fig. 3. Peak deconvolutions of the XPS C1s spectra. (a) CNF–OX, (b) CNF–OH, (c) CNF–CO, and (d) CNF–ON.

assigned to carboxyl groups, than CNF–CO (18.29%) and CNF–OH (16.32%). The C=O groups are apparently converted to C–O groups after reducing with $LiAlH_4$, as the intensity of peak 2 increased while that of peak 3–5 decrease in C1s spectra.

3.3. Cyclic voltammetry of oxygen reduction

Cyclic voltammetry technique was performed to access the electrocatalytic activity of the CNFs toward ORR. As shown in Fig. 5,

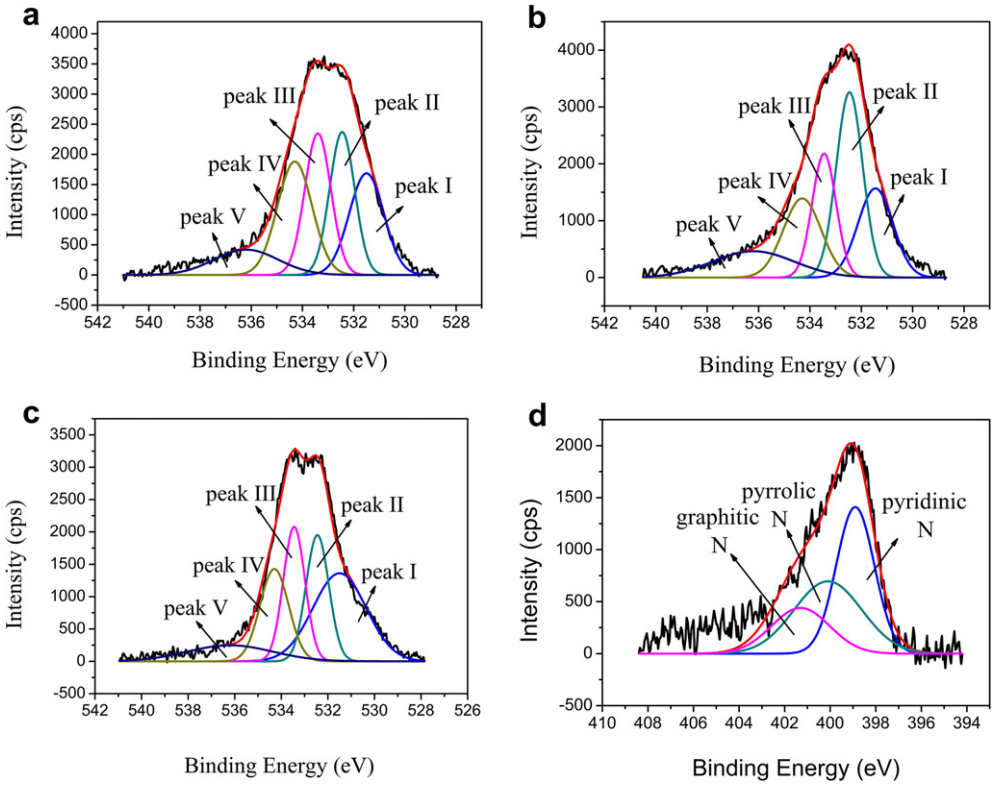

Fig. 4. Peak deconvolutions of the O1s spectra. (a) CNF–OX, (b) CNF–OH, (c) CNF–CO and (d) the N1s spectra of CNF–ON.

Table 2
Relative contents of functional groups obtained from peak deconvolutions of the C1s spectra and the O/C ratio.

Sample	O/C	C1s (%)				
		Peak 1	Peak 2	Peak 3	Peak 4	Peak 5
CNF–P	0.0147	–	–	–	–	–
CNF–OX	0.109	63.64	18.67	5.39	8.17	4.13
CNF–OH	0.0995	66.62	23.29	4.03	3.67	2.39
CNF–CO	0.0953	63.23	18.06	8.83	4.89	2.98
CNF–ON	0.0360	61.86	26.69	4.23	2.99	4.23

the CNF modified GC electrodes were performed in O_2-saturated 0.1 M KOH solutions within the potentials ranging from 0.2 V to −1.2 V under a scanning rate of 10 mV s^{-1}. All the CNF/GC electrodes have an obvious reduction peak within the potentials ranging from −0.2 V to −0.4 V, which can be contributed to a two-electron reduction process of O_2 reduced to HO_2^- [39]. At more negative potentials (from −0.7 V to −0.9 V), an obvious reduction peak is found in the CNF–OX/GC, CNF–OH/GC and CNF–CO/CNF electrodes, which can be associated with a two-electron reduction process of HO_2^- reduced to OH^-, while no clear reduction peak is found in CNF–P/GC and CNF–ON/GC electrodes, which may be due to either the chemical decomposition of HO_2^- or further reduction to form water within the potentials ranging from −0.2 V to −0.4 V [40].

The values of the peak potential (E_P) and peak current density (j_P) on the forward scans as well as the onset reduction potential (E_{OP}) of the CNF/GC electrodes, which reflect the electrocatalytic activity of the catalysts for ORR, were listed in Table 4. We can conclude that the CNF–ON/GC electrode exhibits the highest peak current density (−0.788 mA cm^{-2}) and the most positive onset reduction potential (−0.134 V), so the catalytic activity toward ORR for the CNF–ON/GC electrode is significantly better than that of the rest four electrodes. The excellent electrocatalytic activity of the CNF–ON/GC electrode can be attributed to the incorporation of nitrogen atoms into the graphene layers, which increases the reactivity of the neighborly linked carbon atoms via changing the electronic structure [41], so the CNF–ON/GC electrode has a faster reaction kinetics with a higher transferred electron number per oxygen molecule [42]. The peak potential of the CNF–OX/GC electrode (−0.254 V) is also slightly more positive than CNF–CO/GC electrode (−0.264 V) and CNF–OH/GC electrode (−0.281 V). While all the electrodes exhibit much more positive peak potentials than CNF–P/GC electrode (−0.344 V).

As show in the Raman spectra and CV test, the CNF–OX exhibits slightly less defect sites than CNF–OH and CNF–CO, but the ORR activity is higher than the other two CNFs. The results indicate that the improvement of ORR activity is mainly due to the increasing of functional groups, not the defects. And we can find that the nitrogen-containing groups exhibit the strongest electrocatalytic activity toward ORR, followed by the carboxyl groups, carbonyl groups and hydroxyl groups.

Table 3
Relative contents of functional groups obtained from peak devolutions of the O1s spectra.

Sample	O1s (%)				
	Peak I	Peak II	Peak III	Peak IV	Peak V
CNF–OX	21.47	21.89	22.62	24.08	9.95
CNF–OH	17.35	33.1	22.38	16.32	10.86
CNF–CO	32.37	19.83	20.11	18.29	9.41

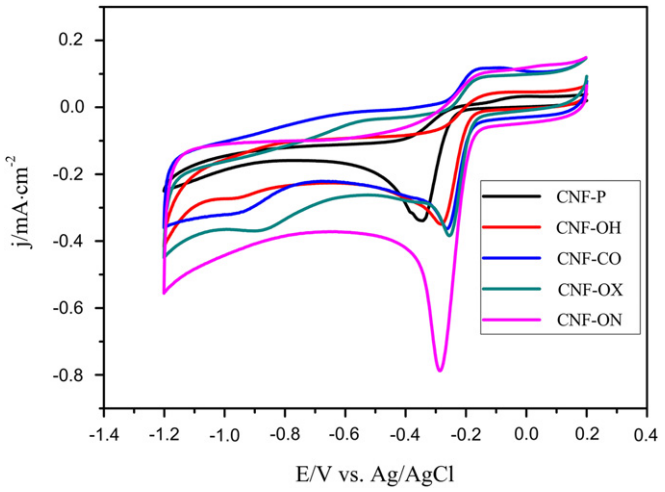

Fig. 5. Cyclic voltammetry curves of ORR on modified CNF/GC electrode in O_2-saturated 0.1 M KOH solutions at a scan rate of 10 mV s^{-1}.

3.4. Rotation disk electrode for oxygen reduction

To get better understanding of the ORR route, the linear sweep voltammetry measurements were performed for the five modified CNF/GC electrodes in O_2-staturated 0.1 M KOH solution. The tests were carried out within the potentials ranging from 0.0 V to −1.2 V under a scanning rate of 10 mV s^{-1}, and the results are shown in Fig. 6. The RDE results for all electrodes are rather similar. The limiting current densities increase with increasing rotating rate, and there are clear reduction peaks at low potentials for all electrodes. The second reduction peaks on the CNF–P/GC, CNF–OX/GC, CNF–CO/GC and CNF–OH/GC electrodes are at approximately −0.8 V, while no obvious reduction peak on the CNF–ON/GC electrode in the same potential. As can be seen in Fig. 6, the higher reduction current density is observed for CNF–OX/GC, CNF–OH/GC, CNF–CO/GC and CNF–ON/GC electrodes than that for the CNF–P/GC electrode, which is probably because of the oxygen- and nitrogen-containing groups on the surface of the treated-CNF. Many studies have found that the oxygen- and nitrogen-containing groups can provide active sites for ORR, and thus effectively increase the electrocatalytic activity toward ORR [43,44].

In order to further explore the ORR mechanism, the RDE data were analyzed using the Koutecky–Levich (K–L) equation [45]:

$$\frac{1}{j} = \frac{1}{j_k} + \frac{1}{j_d} = -\frac{1}{nFkC^b_{O_2}} - \frac{1}{0.62nFD^{2/3}_{O_2}\nu^{-1/6}C^b_{O_2}\omega^{1/2}} \quad (1)$$

Where j is the measured current density, j_k and j_d are the kinetic and diffusion-limited current densities, respectively, n is the number of electrons transferred per O_2 molecule, k is the rate constant for O_2 reduction, F is the Faraday constant (96485 C mol^{-1}), D_{O_2} is the diffusion coefficient of oxygen (1.9×10^{-5} cm^2 s^{-1}) [46], υ is the kinematic viscosity of the solution

Table 4
Electrochemical data for five modified CNF/GC electrodes.

Sample	E_{OP} (V)	E_P (V)	j_P (mA cm^{-2})	n @0.6 V K–L plot
CNF–P	−0.222	−0.344	−0.339	2.11
CNF–OX	−0.144	−0.254	−0.384	2.43
CNF–OH	−0.166	−0.281	−0.350	2.19
CNF–CO	−0.144	−0.264	−0.363	2.35
CNF–ON	−0.134	−0.286	−0.788	3.25

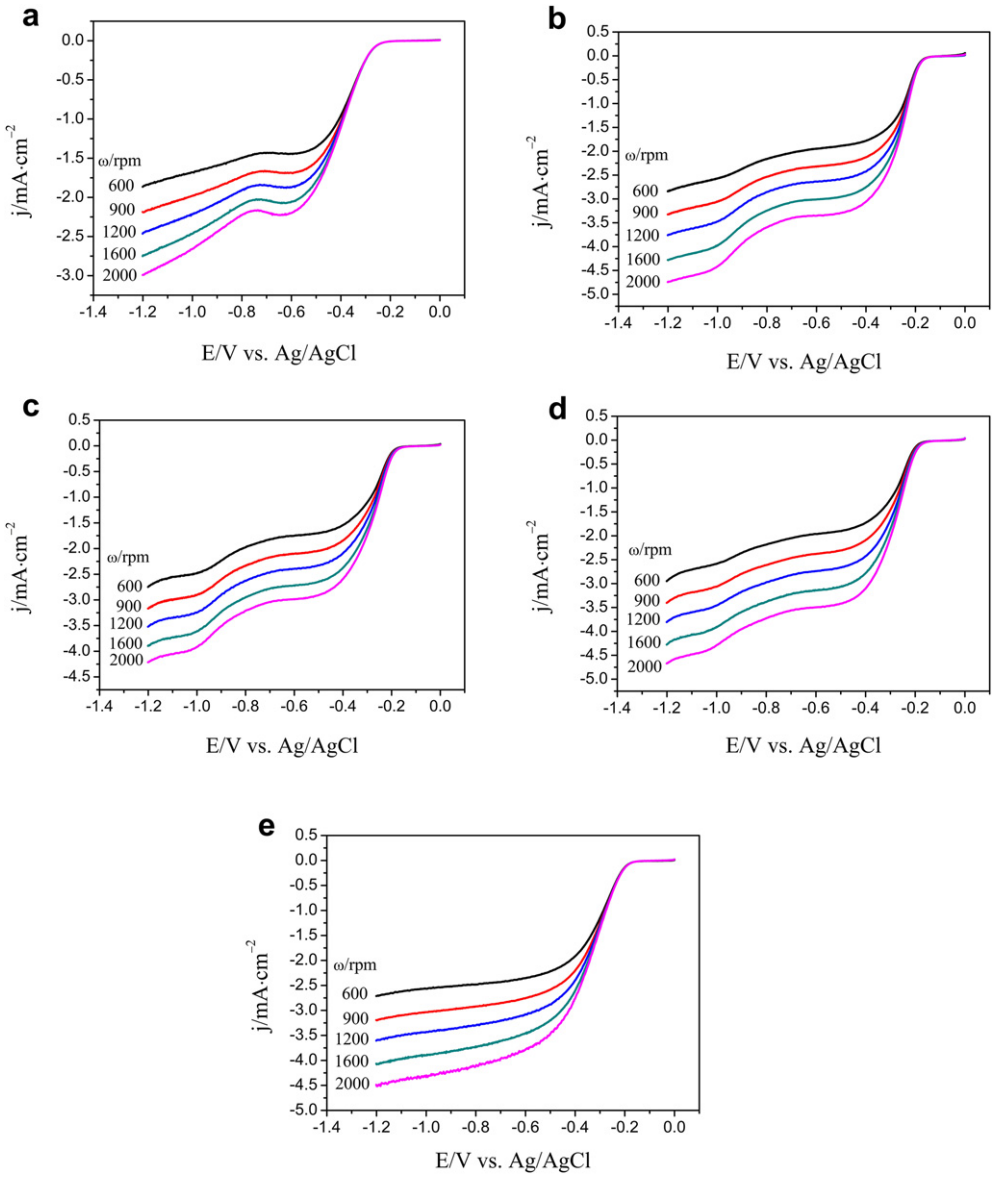

Fig. 6. RDE voltammetry curves for oxygen reduction on carbon modified GC electrodes in O_2-saturated 0.1 M KOH solution. (a) CNF, (b) CNF–OX, (c) CNF–OH, (d) CNF–CO, (e) CNF–ON. $\nu = 10$ mV s^{-1}.

(0.01 cm^2 s^{-1}) [40], $C^b_{O_2}$ is the concentration of oxygen in the bulk (1.13×10^{-6} mol cm^{-3}) [46], and ω is the rotation rate.

Fig. 7 shows the K–L plots obtained from the RDE data of oxygen reduction at −0.6 V for different modified CNF/GC electrodes. At this potential, the K–L lines of CNF–P/GC, CNF–OX/GC, CNF–OH/GC and CNF–CO/GC electrodes are almost parallel, indicating that the reduction pathway is similar for the above four electrodes, while a slightly slower slope ($n = 3.25$) for CNF–ON/GC electrode is found. The intercepts of the extrapolated K–L lines are close to zero, which proves that the process of O_2 reduction is almost entirely under diffusion control. The inset of Fig. 7 compares the n values calculated from the K–L equation at various potentials. For CNF–P/GC, CNF–OX/GC, CNF–OH/GC and CNF–CO/GC electrodes, the n value is close to two at low potentials ($E > -0.6$ V), indicating that in this case the reduction of oxygen produces peroxide. At more negative potentials, the n values of CNF–OX/GC, CNF–OH/GC and CNF–CO/GC electrodes gradually increase to four (the only exception is CNF–P/GC electrode, whose n value remains two), which indicates that the hydrogen peroxide is further reduced to water in this range of potentials. This is in agreement with the previous studies [47]. While the n value of CNF–ON/GC electrode is close to four within the whole range of potential studied, indicating that the reduction of oxygen proceeds predominantly by the four-electron pathway.

There are two typical adsorption modes for an oxygen molecule, the side-on mode (known as the Yeager model) and the end-on mode (known as the Pauling model) [48]. The oxygen molecule is adsorbed by the side-on mode on the CNF–ON catalyst. Both the two oxygen atoms are adsorbed at the C active sites which possesses a high positive charge density adjacent to the N atom (Fig. 8) [39]. The adsorbed oxygen molecule gets 4e$^-$ to release OH$^-$ by breaking the O–O bond. In the whole ORR process, the CNF–ON electrode catalyzes ORR in a four-electron pathway to produce OH$^-$. Among the oxygen-containing groups, the oxygen molecule is adsorbed by the end-on mode which is benefit for catalyzing ORR

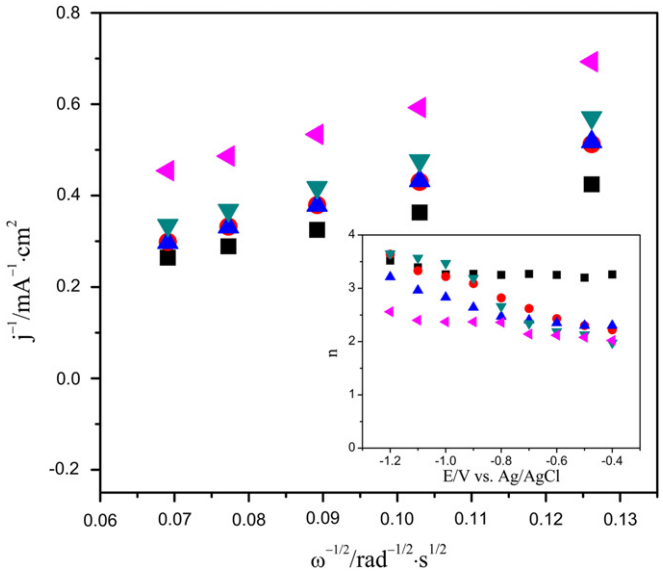

Fig. 7. Koutecky–Levich plots for oxygen reduction on modified CNF GC electrodes at −0.6 V in 0.1 M KOH solution. (■) CNF–ON/GC electrode, (●) CNF–OX/GC electrode, (▲) CNF–CO/GC electrode, (▼) CNF–OH/GC electrode, (◀) CNF/GC electrode. The inset shows the dependence of *n* on potential.

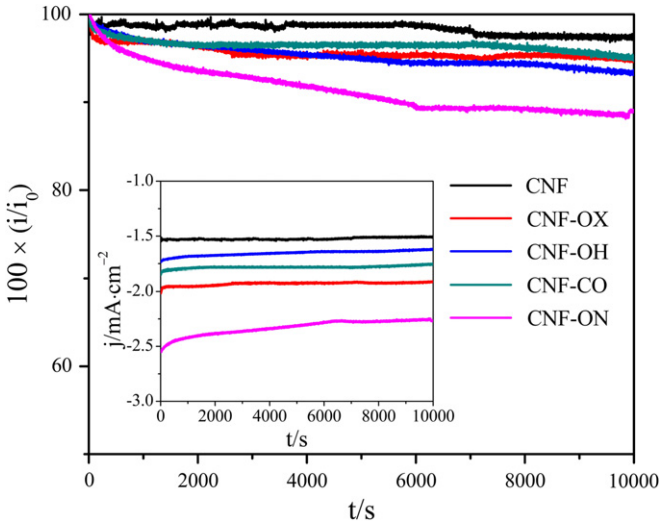

Fig. 9. Chronoamperometric responses (percentage of current retained versus operation time) of CNF–P, CNF–OX, CNF–OH, CNF–CO and CNF–ON electrodes at −0.6 V in an O_2-saturated 0.1 M KOH at a rotation speed of 600 rpm. The inset shows the current–time curves of the five electrodes.

in a two-electron pathway to produce HO_2^- (Fig. 8). The carbon atom in carbonyl group has a relatively strong electropositive, which is beneficial to adsorbing an oxygen atom of the oxygen molecule, so the CNF–CO electrode exhibits higher ORR activity compared with CNF–OH electrode. Although the electropositive of the C atom in carboxyl group is weaker than that in carbonyl group, the ORR activity of CNF–OX electrode exhibits higher than CNF–CO electrode, it is possible that the oxygen anion in carboxyl group could synergistically bonds with oxygen molecule when the oxygen molecule is absorbed to the C active site, so carboxyl group can weaken the CNF–O bond more easily and exhibit the highest ORR activity. However, the detailed mechanism is still unclear. All the oxygen-containing groups can be easily bonded with H_2O_2, thus it is favorable for further reduction of H_2O_2 to H_2O. So that the *n* value of CNF–OX/GC, CNF–OH/GC and CNF–CO/GC electrodes (near four) are higher than that of CNF–P/GC electrode (which remains near two) at the potentials ranging from −1.0 V to −1.2 V.

3.5. Chronoamperometry (CA)

CA is usually employed to check the stability of CNF catalysts for ORR [49,50]. The stability tests for five catalysts towards ORR have been carried out by the CA technique at a potential of −0.6 V in O_2-saturated 0.1 M KOH at a rotation speed of 600 rpm. Before the CA test, the catalysts are activated by RDE test for two cycles. The corresponding results are shown in Fig. 9. As expected, the CNF–ON catalyst demonstrates the highest current density for ORR. Values of current density for ORR measured after 10000s are −2.27, −1.91, −1.72, −1.62 and −1.51 mA cm^{-2} on CNF–ON, CNF–OX, CNF–CO, CNF–OH and CNF–P catalysts, respectively. The current from the five electrodes hardly decrease with the increase of time. Obviously, all the five catalysts exhibit good stability for ORR.

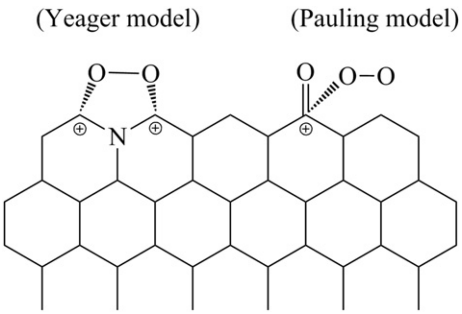

Fig. 8. The oxygen adsorption models towards ORR.

4. Conclusions

By using different treatment methods, CNF–P, CNF–OX, CNF–OH, CNF–CO and CNF–ON have been obtained in this work. The application of the CNF modified electrode in the electrochemical reduction of oxygen has been studied by CV and RDE tests. The results of the present research indicate that both oxygen- and nitrogen-containing groups are effective to increase the electrocatalytic activity of CNF toward ORR in alkaline solution. For all the functional groups on CNF surface, the nitrogen-containing groups have the strongest electrocatalytic activity (−0.788 mA cm^{-2}), followed by the carboxylic acid groups (−0.384 mA cm^{-2}), the carbonyl groups (−0.363 mA cm^{-2}) and the hydroxyl groups (−0.350 mA cm^{-2}). The surface functional groups can also change the ORR pathway. The oxygen reduction of CNF–ON/GC electrode proceeds almost entirely through the four-electron reduction pathway, the CNF–OX/GC, CNF–CO/GC and CNF–OH/GC electrodes proceed a two-electron reduction at low potentials followed by a gradually four-electron reduction at more negative potentials, while the CNF–P/GC electrode catalyze ORR through two-electron pathway within the whole range of potential studied. All the five catalysts exhibit good stability for ORR.

Acknowledgments

The present study was supported by the Nature Science Foundation of China (21073061), the State Key Laboratory of Physical Chemistry of Solid surfaces (Xiamen University), the State Key

Laboratory Breeding Base of Green Chemistry Synthesis Technology (Zhejiang University of Technology), and the 111 Project (B08021).

References

[1] Y.H. Qin, H.H. Yang, X.S. Zhang, P. Li, C.A. Ma, Int. J. Hydrogen Energy 35 (2010) 7667–7674.
[2] Y. Xing, J. Phys. Chem. B 108 (2004) 19255–19259.
[3] T.G. Ros, D.E. Keller, A.J. van Dillen, J.W. Geus, D.C. Koningsberger, J. Catal. 211 (2002) 85–102.
[4] H.T. Zheng, Y. Li, S. Chen, P.K. Shen, J. Power Sources 163 (2006) 371–375.
[5] J. Guo, G. Sun, Q. Wang, G. Wang, Z. Zhou, S. Tang, L. Jiang, B. Zhou, Q. Xin, Carbon 44 (2006) 152–157.
[6] J.S. Zheng, X.S. Zhang, P. Li, J. Zhu, X.G. Zhou, W.K. Yuan, Electrochem. Commun. 9 (2007) 895–900.
[7] I. Kruusenberg, N. Alexeyeva, K. Tammeveski, Carbon 47 (2009) 651–658.
[8] N. Alexeyeva, E. Shulga, V. Kisand, I. Kink, K. Tammeveski, J. Electroanal. Chem. 648 (2010) 169–175.
[9] S. Sotiropoulou, N.A. Chaniotakis, Anal. Bioanal. Chem. 375 (2003) 103–105.
[10] M.L. Toebes, J.M.P. van Heeswijk, J.H. Bitter, A.J. van Dillen, K.P. de Jong, Carbon 42 (2004) 307–315.
[11] J.H. Zhou, Z.J. Sui, J. Zhu, P. Li, D. Chen, Y.C. Dai, W.K. Yuan, Carbon 45 (2007) 785–796.
[12] M. Glerup, J. Steinmetz, D. Samaille, O. Stéphan, S. Enouz, A. Loiseau, S. Roth, P. Bernier, Chem. Phys. Lett. 387 (2004) 193–197.
[13] S. Enouz, O. Stéphan, J.L. Cochon, C. Colliex, A. Loiseau, Nano Lett. 7 (2007) 1856–1862.
[14] S. Maldonado, K.J. Stevenson, J. Phys. Chem. B 109 (2005) 4707–4716.
[15] D.C. Wei, Y.Q. Liu, Y. Wang, H.L. Zhang, L.P. Huang, G. Yu, Nano Lett. 9 (2009) 1752–1758.
[16] Y. Liao, L. Gao, X. Zhang, J. Chen, Mater. Res. Bull. 47 (2012) 1625–1629.
[17] K. Lee, L. Zhang, H. Lui, L. Hui, Z. Shi, J. Zhang, Electrochim. Acta 54 (2009) 4704–4711.
[18] B. Šljukić, C.E. Banks, R.G. Compton, J. Iran. Chem. Soc. 2 (2005) 1–25.
[19] M. Chisaka, T. Iijima, A. Tomita, T. Yaguchi, Y. Sakurai, J. Electrochem. Soc. 157 (2010) 1701–1706.
[20] K. Matsubara, K. Waki, Electrochem. Solid State Lett. 28 (2010) 35–46.
[21] R. Chen, H. Li, D. Chu, G. Wang, J. Phys. Chem. C 113 (2009) 20689–20697.
[22] E.J. Biddinger, D. von Deak, D. Singh, H. Marsh, B. Tan, D.S. Knapke, U.S. Ozkan, J. Electrochem. Soc. 158 (2011) 402–409.
[23] C.E. Banks, T.J. Davies, G.G. Wildgoose, R.G. Compton, Chem. Commun. 7 (2005) 829–841.
[24] K. Gong, S. Chakrabarti, L. Dai, Angew. Chem. Int. Ed. 47 (2008) 5446–5450.
[25] L. Qu, Y. Liu, J.B. Baek, L. Dai, ACS Nano 4 (2010) 1321–1326.
[26] J. Xu, W. Huang, R.L. McCreery, J. Electroanal. Chem. 410 (1996) 235–242.
[27] Y. Jiang, J. Zhang, Y.H. Qin, D.F. Niu, X.S. Zhang, L. Niu, X.G. Zhou, T.H. Lu, W.K. Yuan, J. Power Sources 196 (2011) 9356–9360.
[28] S. Osswald, M. Havel, Y. Gogotsi, J. Raman Spectrosc. 38 (2007) 728–736.
[29] M.K. van der Lee, A.J. van Dillen, J.H. Bitter, K.P. de Jong, J. Am. Chem. Soc. 127 (2005) 13573–13582.
[30] A.J. Plomp, D.S. Su, K.P. de Jong, J.H. Bitter, J. Phys. Chem. C 113 (2009) 9865–9869.
[31] N. Gavrilov, I.A. Pašti, M. Mitrić, J. Travas-Sejdic, G. Ćirić-Marjanovića, S.V. Mentus, J. Power Sources 220 (2012) 306–316.
[32] Z.H. Sheng, L. Shao, J.J. Chen, W.J. Bao, F.B. Wang, X.H. Xia, ACS Nano 5 (2011) 4350–4358.
[33] W. Yang, T.P. Fellinger, M. Antonietti, J. Am. Chem. Soc. 133 (2011) 206–209.
[34] A. Rey, M. Faraldos, A. Bahamonde, Ind. Eng. Chem. Res. 47 (2008) 8166–8174.
[35] H.K. Jeong, Y.P. Lee, R.L.W.E. Lahaye, M.H. Park, K.H. An, I.J. Kim, C.W. Yang, C.Y. Park, R.S. Ruoff, Y.H. Lee, J. Am. Chem. Soc. 130 (2008) 1362–1366.
[36] V. Datsyuk, M. Kalyva, K. Papagelis, J. Parthenios, D. Tasis, A. Siokou, I. Kallitsis, C. Galiotis, Carbon 46 (2008) 833–840.
[37] J.L. Figueiredo, M.F.R. Pereira, Catal. Today 150 (2010) 2–7.
[38] L.G. Bulusheva, A.V. Okotrub, I.A. Kinloch, I.P. Asanov, A.G. Kurenya, A.G. Kudashov, X. Chen, H. Song, Phys. Status Solidi (b) 245 (2008) 1971–1974.
[39] K. Gong, F. Du, Z. Xia, M. Durstock, L. Dai, Science 323 (2009) 760–764.
[40] I. Kruusenberg, J. Leis, M. Arulepp, J. Solid State Electrochem. 14 (2010) 1269–1277.
[41] R. Chetty, S. Kundu, W. Xia, M. Bron, W. Schuhmann, V. Chirila, Electrochim. Acta 54 (2009) 4208–4215.
[42] M. Zhang, Y. Yan, K. Gong, L. Mao, Z. Guo, Y. Chen, Langmuir 20 (2004) 8781–8785.
[43] G. Jürmann, D.J. Schiffrin, K. Tammeveski, Electrochim. Acta 53 (2007) 390–399.
[44] R.A. Sidik, A.B. Anderson, N.P. Subramanian, J. Phys. Chem. B 110 (2006) 1787–1793.
[45] N. Alexeyeva, K. Tammeveski, A. Lopez-Cudero, J. Solla-Gullón, J.M. Feliu, Electrochim. Acta 55 (2010) 794–803.
[46] I. Roche, E. Chaînet, M. Chatenet, J. Vondrák, J. Phys. Chem. C 111 (2007) 1434–1443.
[47] G. Jürmann, K. Tammeveski, J. Electroanal. Chem. 597 (2006) 119–126.
[48] H. Kim, K. Lee, S.I. Woo, Y. Jung, Phys. Chem. Chem. Phys. 13 (2011) 17505–17510.
[49] C. Zhang, R. Hao, H. Liao, Y. Hou, Nano Energy (2012) 1–10.
[50] Y. Liang, Y. Li, H. Wang, J. Zhou, J. Wang, T. Regier, H. Dai, Nat. Mater. 10 (2011) 780–786.